Zero-Shot Scene Change Detection

Kyusik Cho[1]   **Dong Yeop Kim**[1,2]   **Euntai Kim**[1*]
[1]Yonsei University,   [2]Korea Electronics Technology Institute
{ks.cho, etkim}@yonsei.ac.kr, sword32@keti.re.kr

Abstract: We present a novel, training-free approach to scene change detection. Our method leverages tracking models, which inherently perform change detection between consecutive frames of video by identifying common objects and detecting new or missing objects. Specifically, our method takes advantage of the change detection effect of the tracking model by inputting reference and query images instead of consecutive frames. Furthermore, we focus on the content gap and style gap between two input images in change detection, and address both issues by proposing adaptive content threshold and style bridging layers, respectively. Finally, we extend our approach to video to exploit rich temporal information, enhancing scene change detection performance. We compare our approach and baseline through various experiments. While existing train-based baseline tend to specialize only in the trained domain, our method shows consistent performance across various domains, proving the competitiveness of our approach.

Keywords: Scene Change Detection, Zero-shot learning

1 Introduction

Scene Change Detection (SCD) is the task that aims to detect differences between two scenes separated by a temporal interval, and it is a fundamental capability required for mobile robots to ensure reliable navigation, and task performance completion. If a robot lacks the capability of SCD, several problems could arise, affecting its performance, safety, and overall effectiveness. Without SCD, for instance, a robot might not be able to detect recently added barriers or changes in the environment, which could result in collisions and possible harm to the robot as well as other objects. Furthermore, without the capability of SCD, the robot's maps of the environment would not be updated frequently enough, reducing the accuracy of localization and navigation tasks. This can lead to increased errors in estimating its position. Conversely, robots equipped with SCD capabilities can be employed in various applications, such as disaster detection [1, 2], terrain monitoring [3, 4, 5], and industrial warehouse management [6, 7].

Recently, SCD has been tackled using deep learning. Deep learning-based SCD techniques follow a procedure of learning from a training dataset and applying the model to a test dataset. These approaches tend to face two main challenges: dataset generation costs and susceptibility to style variations. Firstly, creating a training dataset for SCD models is labor-intensive and costly. Recent research has focused on reducing these costs through semi-supervised [8, 9] and self-supervised learning [10, 11] methods, as well as the use of synthetic data [12, 8]. While these approaches mitigate the expense of labeling, they often overlook the cost of acquiring image pairs and fail to address the unnaturalness of collecting such data, as humans typically do not need image pairs for change detection. Secondly, due to the substantial temporal intervals between pre-change and post-change images, variations in seasons, weather, and time introduce significant differences in their visual characteristics. Consequently, SCD techniques must be robust to these style variations to be effective. However, the training dataset cannot include all the style variations present in real-world scenarios, making the trained model vulnerable to style variations that are not included in the training set.

---

*Corresponding author

To address these problems, we propose a novel training-free zero-shot SCD method. Our method does not require a training dataset, thereby eliminating collection costs and allows it to be applied to any problem with arbitrary styles. To the best of our knowledge, this paper is the first to attempt zero-shot SCD without training on a training dataset. The key idea of this paper is to formulate SCD as a tracking problem, and apply a foundation tracking model to conduct zero-shot SCD. This idea stems from the observation that the tracking task is fundamentally similar to change detection. Specifically, tracking models [13, 14] maintain or build tracks by identifying the same objects, disappeared objects, and newly appeared objects in two consecutive images, even when the camera and objects move. Thus, if the two consecutive images in tracking are replaced with the two images before and after the change in SCD, the tracking model can automatically solve SCD without training.

However, it is worth noting that there are some differences between tracking and SCD: (a) Unlike tracking, the two images before and after the change in SCD might have different styles due to a large time gap between two images. We refer to this SCD trait as the style gap. (b) Objects change very little between two consecutive images in tracking, whereas objects change abruptly in SCD. We refer to this SCD trait as the content gap. To address these issues in our zero-shot SCD method, we introduce a style bridging layer and a content threshold, respectively.

Finally, we extend our approach to sequence, to introduce the zero-shot SCD approach works on the video. Since our approach operates based on a tracking model, it can be seamlessly extended to work with video sequences. The proposed zero-shot SCD approach has been evaluated on three benchmark datasets and shows that our zero-shot SCD demonstrates comparable or even superior performance compared to previous state-of-the-art training-based SCD methods.

2   Related Work

Scene Change Detection (SCD): In recent years, numerous deep learning-based change detection methods have been proposed for SCD. DR-TANet [15] utilized attention mechanism based on the encoder-decoder architecture. SimSaC [7] developed a network with a warping module to correct distortions between images. C-3PO [16] developed a network that fuses temporal features to distinguish three change types. However, various studies have aimed to address the challenge of obtaining data. For instance, [8, 9] have introduced semi-supervised learning, and [10, 11] proposed the self-supervised learning with unlabeled data. However, [12, 8] utilized synthetic data to effectively increase the dataset. Despite these methods effectively reducing the label costs, they tend to overlook the cost of collecting image pairs. Moreover, the robustness against style change has not been previously discussed. An effective SCD method should be able to focus on content changes regardless of variations in image style. However, since a single dataset cannot encompass all possible style variations, the performance tends to be specialized for the styles present in the dataset. This issue, while not evident in controlled laboratory environments, becomes a significant problem in real-world applications. Therefore, we propose a novel SCD method that does not rely on datasets. Our method operates without a training dataset, thus ensuring independence from specific styles.

Segmenting and Tracking Anything: Recently, Segment Anything [17] has demonstrated highly effective performance in universal image segmentation. SAM has shown the ability to perform various zero-shot tasks, and has served as the foundational model for various studies [18, 19]. Building upon this research, researchers have explored various methods to extend its application to tracking. For example, SAM-Track [20] implemented tracking by combining SAM with the DeAOT [21] mask tracker. SAM-PT [22] integrated SAM with point tracking to develop the pipeline. DEVA [13] proposed a pipeline that uses the XMem tracker [14] to track provided masks without additional training. Among various studies, we adopted DEVA with SAM masks as our tracking model, to achieve track-anything for SCD without further training.
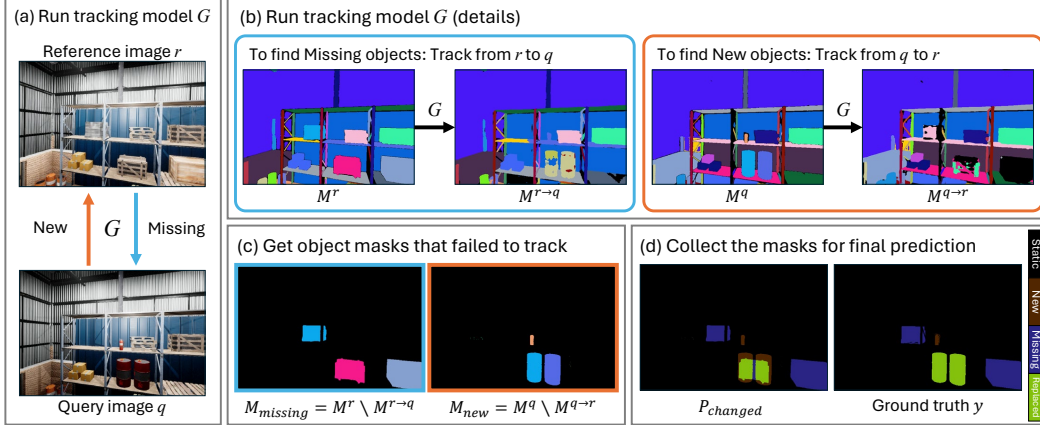
Figure 1: **The Basic idea of SCD with tracking model.** (a) We execute the tracking model G with r and q. (b) We denote the tracking result from r to q as $M^{r \to q} = G(r, q, M^r)$, and the tracking result from q to r as $M^{q \to r} = G(q, r, M^q)$ (c) 'Missing' objects are the objects that exist in r but not in q. Therefore, we compare M^r and $M^{r \to q}$ to find missing objects. Conversely, 'new' objects are identified by comparing M^q and $M^{q \to r}$. (d) The final prediction is the simple combination of new and missing.

3 Method

Each datum for scene change detection (SCD) is represented as a triplet (r, q, y), where r and q denote paired images acquired at distinct times t_0 and t_1, respectively, and y represents the change label between the image pair. The primary objective of this task is to discern the scene change between the images captured at t_0 and t_1 when inspecting the latter. Herein, we call the image obtained at t_0 (r) as the reference image and the image acquired at t_1 (q) as the query image.

To perform scene change detection without training, our methodology integrates two pretrained models: a segmentation model F and a tracking model G. The segmentation model F segments images in an unsupervised manner, while the tracking model G tracks each mask generated by F across multiple images. We employ the Segment Anything Model (SAM) [17] as the segmentation model F and DEVA [13] for the tracking model G. Comprehensive details about parameters for F and G, and details about mask generation process will be provided in the supplementary materials.

We first introduce the basic idea for performing SCD between two images using F and G in Section 3.1. Next, we discuss the differences between the tracking task and the SCD task, and then introduce methods to overcome these differences in Section 3.2. Finally, we extend our approach to the video level in Section 3.3.

3.1 Scene Change Detection with Tracking model

Our approach uses two pretrained models, a segmentation model F and a tracking model G. The segmentation model F partitions image I into object-level masks, forming the set $M = \{m_0, m_1, \cdots, m_n\}$. There exists no overlap between distinct masks, that is, $m_i \cap m_j = 0, \forall i \neq j$. The tracking model G takes consecutive frame images (I^0, I^1) and the object masks of the first frame $M^0 = F(I^0)$ as input, and yields $M^{0 \to 1}$ as output, that is, $M^{0 \to 1} = G(I^0, I^1, M^0)$. Here, $M^{0 \to 1}$ represents the set of masks tracked from $M^0 = F(I^0)$ to I^1. By checking if each mask that was present in M^0 is also present in $M^{0 \to 1}$, we can see which masks still exist and which ones have disappeared from I^0 and I^1.

The key idea of our zero-shot SCD is to apply a reference frame r and a query frame q instead of consecutive frames (I^0, I^1) to the tracking model G. Although the tracking model traditionally expects consecutive frames (I^0, I^1) for input, we deviate from this convention by providing reference frame r and query frame q instead. To avoid potential confusion, we rewrite the input and the output

3

of the tracking model as $M^{r \to q} = G(r, q, M^r)$. By comparing the masks between M^r and $M^{r \to q}$, we identify object masks that exist at time t_0 but have disappeared at time t_1, corresponding to the 'missing' class in the change detection task. Specifically,

$$M_{missing} = M^r \setminus M^{r \to q}. \tag{1}$$

Additionally, we run the tracking model G again by reversing the order reference frame r and query frame q and feed them to G to obtain $M^{q \to r} = G(q, r, M^q)$. Similarly, we predict the 'new' objects by $M_{new} = M^q \setminus M^{q \to r}$, which represent the objects that appear at time t_1 but were absent at time t_0. Our pixel-wise prediction is obtained by applying the union of masks within M_{new} and $M_{missing}$. Pixels experiencing both 'new' and 'missing' occurrences are considered 'replaced.' Formally, change prediction $P_{changed}$ is determined by:

$$
\begin{aligned}
P_{missing} &= \bigcup M_{missing} \\
P_{new} &= \bigcup M_{new} \\
P_{replaced} &= P_{missing} \cap P_{new} \\
P_{changed} &= P_{missing} \cup P_{new}
\end{aligned}
\tag{2}
$$

The entire process of this approach is illustrated in Figure 1.

3.2 Addressing Content Gap and Style Gap

As presented in Section 3.1, the key idea of our zero-shot SCD is to exploit the similarity between SCD and tracking tasks. However, directly applying this concept to various SCD scenarios can sometimes result in performance degradation due to inherent differences between the two tasks. In this section, we examine these differences and propose corresponding solutions.

The first difference is the content gap, which refers to abrupt changes in content between the reference and query images. In traditional tracking tasks, objects typically disappear gradually over multiple frames rather than suddenly, and new objects appear gradually over multiple frames, implying that tracking tasks have little content gap. In contrast, SCD involves abrupt changes where objects disappear or appear within a single frame and it has a large content gap. Therefore, when the tracking model G trained on the tracking dataset is directly applied to SCD, the tracking model G tends to create small segments even for objects that have disappeared, as shown in Figure 2. In the first row, the yellow forklift in the query image is missing from the reference image, but, in the second row, the mask in $M^{q \to r}$ tracked from a blue mask in M^q has a small segment. This remaining small segment from the tracking model G makes the identification of missing objects very difficult.

To address the problem, when the size of an object is significantly reduced after the tracking, we consider the object has disappeared even if its size is not completely vanished. To the end, we intro-

Figure 2: **Illustration of Content Threshold.** Since the yellow forklift in q has disappeared in r, all the three masks (blue, red, and yellow masks) in M^q have no associated masks in $M^{q \to r}$. However, the tracking model creates a small area of the blue mask in $M^{q \to r}$ due to the content gap. This makes it mistakenly classified as a static object. To address this, we propose a content threshold to filter out masks whose area significantly reduces after tracking.

duce a content threshold τ and we compare the areas of the masks before and after tracking. If the ratio is less than the content threshold τ, we consider the corresponding object is missing or newly
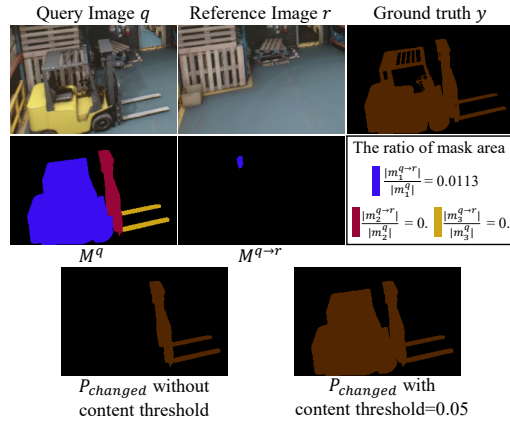
4

appeared. We define the $\setminus^\tau$ operator to replace the $\setminus$ operator in equation 1 as follows, where $|m_i^*|$ denotes the area of the i-th mask in set *:

$$A \setminus^\tau B := \{m_i^A \mid \frac{|m_i^B|}{|m_i^A|} < \tau, \quad \forall m_i^A \in A\}. \tag{3}$$

By introducing this operator, we have $M_{missing} = M^r \setminus^\tau M^{r \to q}$. The value of τ is set to 0.05.

The second difference between tracking tasks and SCD is the style gap, which refers to the difference in style between the reference and query images. This style gap arises in SCD because there is a long time interval between the capture of the reference image and the query image, during which weather, time of day, or even season can change. Such variations are not considered in traditional tracking tasks and it can significantly degrade the SCD performance.

To address the style gap, we introduce a style bridging layer (SBL) by incorporating an Adaptive Instance Normalization (AdaIN) layer [23] into the residual blocks of ResNet backbone [24]. The AdaIN layer, widely used to reduce style differences between images across various fields [25, 26, 27], references the first image and applies its style to the second image, thereby reducing the style differences between the two images. Inspired by this, SBL addresses the style gap between two inputs without learning, with two training-free style parameters. For example, during the process $M^{r \to q} = G(r, q, M^r)$, the style bridging layer

Figure 3: **Illustration of Style Bridging Layer.** During the processing of the first image, the style is saved while the feature is passed through unchanged. When processing the second image, the saved style is applied to the feature.

records the mean and variance of each layer in image r and applies these statistics when processing image q. Formally, the style bridging layer updates the feature of z_l^q as follows, where z_l^* denotes the l-th layer feature of image *.

$$\tilde{z}_l^q = \sigma(z_l^r) \frac{z_l^q - \mu(z_l^q)}{\sigma(z_l^q)} + \mu(z_l^r). \tag{4}$$

The operation of the proposed style bridging layer is illustrated in Figure 3.

Through these two methods, we effectively and simply address the content gap and style gap. Note that the two improvements are also applied in the process $M^{q \to r} = G(q, r, M^q)$ and $M_{new} = M^q \setminus^\tau M^{q \to r}$.

3.3 Extension to the Video Sequences

In this subsection, the SCD between two images is extended to the SCD between two videos. Using the tracking model enables us to seamlessly extend image SCD to video SCD. Consider a video SCD dataset consisting of sequences of reference, query, and change labels, denoted as $\{r^t, q^t, y^t\}_{t=1}^T$, where T represents the length of the video sequence, and t denotes the time index. Utilizing the videos in SCD provides a richer representation of the objects and improves the SCD performance. Compared to the image SCD, the video SCD requires three modifications. The first modification is simply to feed two sequences $\{r^t, q^t\}_{t=1}^T$ instead of image pair $\{r, q\}$ as input to the tracking model. Specifically, we start the video SCD with

$$
\begin{aligned}
M^{r^1 \to r^2} &= G(r^1, r^2, M^{r^1}) \\
M^{r^1 \to r^2 \to q^2} &= G(r^2, q^2, M^{r^1 \to r^2}),
\end{aligned} \tag{5}
$$

and proceed with our SCD by

$$
\begin{aligned}
M^{r^1 \twoheadrightarrow r^t} &= G(r^{t-1}, r^t, M^{r^1 \twoheadrightarrow r^{t-1}}) \\
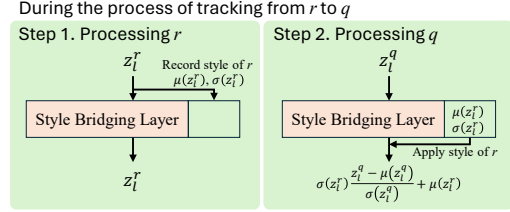M^{r^1 \twoheadrightarrow q^t} &= G(r^t, q^t, M^{r^1 \twoheadrightarrow r^t}),
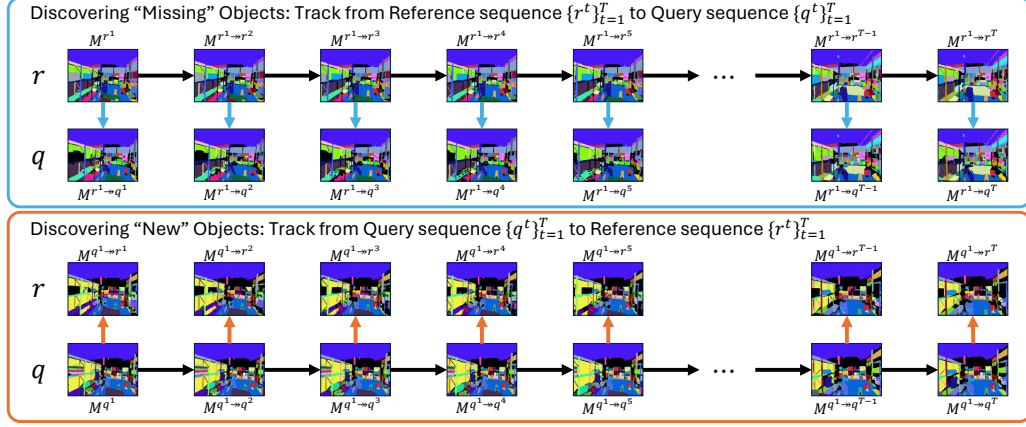\end{aligned} \tag{6}
$$

Figure 4: **Zero-Shot SCD in video.** We conduct SCD on video sequences by providing sequence pairs instead of image pairs as input to the tracking model G. For each frame, the mask is propagated from the previous frame, resulting in a mask sequence through repeated propagation. SCD in the video is finalized by comparing the mask sequences.

where $M^{r^1 \twoheadrightarrow r^t} = M^{r^1 \to r^2 \to \cdots \to r^{t-1} \to r^t}$ and $M^{r^1 \twoheadrightarrow q^t} = M^{r^1 \to r^2 \to \cdots \to r^{t-1} \to r^t \to q^t}$, as shown in Figure 4. In mask formulation, M^X denotes the output from the segmentation model F, whereas $M^{X \to Y}$ or $M^{X \twoheadrightarrow Y}$ denotes the output from tracking model G. This architecture is slightly similar to the structure of the Bayes filters or Markov process [28], in that all the information processed from 1 to $t-1$ are included in $M^{r^1 \twoheadrightarrow r^{t-1}}$. Consequently, $M^{r^1 \twoheadrightarrow r^t}$ can be incrementally updated from $M^{r^1 \twoheadrightarrow r^{t-1}}$ and r^t, q^t, without reprocessing all previous images. During the incremental update from $M^{r^1 \twoheadrightarrow r^{t-1}}$ to $M^{r^1 \twoheadrightarrow r^t}$, all functions for tracking, including updating feature memory and discovering new objects, are activated. Conversely, during the update from $M^{r^1 \twoheadrightarrow r^t}$ to $M^{r^1 \twoheadrightarrow q^t}$, these functions are deactivated. This processing sequence is designed to detect missing objects, whereas the opposite processing sequence with swapping r and q is employed to detect new objects.

The second modification is to define $M^t_{missing}$ and M^t_{new} at time t. To find missing objects, we consider all frames in query sequence $\{q^t\}^T_{t=1}$, as follows:

$$M^t_{missing} = \{M^{r^t} \setminus^\tau M^{r^1 \twoheadrightarrow q^1}\} \cap \{M^{r^t} \setminus^\tau M^{r^1 \twoheadrightarrow q^2}\} \cap \cdots \cap \{M^{r^t} \setminus^\tau M^{r^1 \twoheadrightarrow q^T}\}. \quad (7)$$

This definition of $M^t_{missing}$ indicates that the missing object is the object that exists in reference frame r^t, but is absent in the query sequence $\{q^t\}^T_{t=1}$. M^t_{new} is similarly defined with the object that exists in query frame q^t, but is absent in the reference sequence $\{r^t\}^T_{t=1}$.

However, with more cross-sequence comparisons, there is a higher noise exposure. Therefore, as the sequence length increases, it becomes necessary to adjust the content threshold introduced in Section 3.2. The third modification is extending it to an adaptive content threshold based on the sequence length, defined by the following equation:

$$\tau = 0.5 - \frac{0.9}{\sqrt{length + 1}}. \quad (8)$$

As the sequence length increases, the threshold becomes higher. The threshold is capped at 0.5.

Through these three extensions, our methodology becomes appropriate for processing videos. According to the definitions of these three modifications, the sequence length can range from 1 to infinity. However, we impose an upper bound on the length of a sequence, denoted as T_{max}. If the length of the video exceeds T_{max}, it is treated as multiple sequences each with a length of T_{max} individually. The reason for constraining the length of sequences is simple: as sequences lengthen, memory costs increase, while the relevant information for change detection diminishes. For instance, in scenarios where the camera is in motion, the initial and final frames of a sequence may capture entirely different locations, rendering them unsuitable for change detection. Conversely, if

ChangeSim: In-domain							
Method	Trained Set	Test Set	Static	New	Missing	Replaced	mIoU
C-3PO [16]	Normal	Normal	94.2	14.3	5.3	17.1	32.7
Ours	-		93.9	29.6	12.3	7.3	**35.8**
C-3PO	Dust	Dust	94.0	9.3	2.8	12.6	29.7
Ours	-		88.6	23.2	6.4	8.1	**31.6**
C-3PO	Dark	Dark	93.8	5.4	0.6	8.4	**27.1**
Ours	-		80.6	9.4	4.7	6.3	25.2

Table 1: **Experimental results.** Results are expressed in per-class IoU and mIoU scores. Despite the absence of a training process, our model outperformed the baseline's in-domain performance in two out of three subsets.

ChangeSim: Cross-domain				
			Test set	
Method	Trained Set	Normal	Dust	Dark
	Normal	32.7	27.2	26.7
C-3PO	Dust	29.6	29.7	26.9
	Dark	29.4	27.1	**27.1**
Ours	-	**35.8**	**31.6**	25.2

Table 2: **Experimental results on cross-domain.** Results are expressed in the mIoU score across all change classes. We trained the baseline model on each subset and tested it across all subsets. The experimental results show that the baseline model achieves the highest performance when the training set and test set are the same, while performance degrades when the training and test sets differ. In contrast, our method is free from this issue.

the camera remains stationary, all frames depict the same scene, and redundant frames do not contribute useful information. Therefore, we ensure more effective SCD by setting the upper bound of the sequence length. For our experiments, we set T_{max} to 60.

4 Experiments

4.1 Experimental Setup

In this section, we briefly introduce the dataset, the relevant settings, and the evaluation metrics.

ChangeSim [6] is a synthetic dataset with an industrial indoor environment. It includes three subsets with varying environmental conditions: normal, low-illumination, and dusty air. The dataset categorizes changes into four types: new, missing, rotated, and replaced. Despite its variety of environmental variations and change classes, most baseline experiments on this dataset have evaluated only the binary change/unchange classification and have predominantly focused on the normal subset, leaving the dataset's full potential underexplored. Therefore, we chose the state-of-the-art method, C-3PO [16], and reproduced the results under the following conditions: using the original image size (640×480) to fully utilize the rich information; and including all three subsets. Among the four change classes in this dataset, the rotated class, unlike others, involves slight angular changes of the same object rather than complete appearances or disappearances. We considered this as the object remaining static and integrated this class into static for evaluation.

Evaluation Metrics. We employ the mean Intersection over Union (mIoU) metric.

4.2 Experimental Results

Table 1 presents the experimental results with other state-of-the-art, C-3PO [16] from ChangeSim. C-3PO is reproduced under the conditions described in Section 4.1. The baseline model is tested
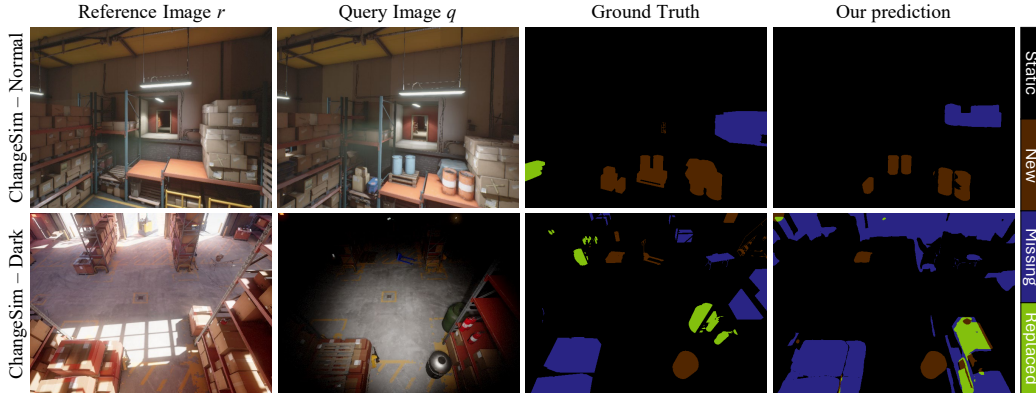
Figure 5: **Qualitative Results.** Our approach successfully performs change detection across various datasets without training.

on the same datasets as its training dataset, denoted as in-domain. The table shows that our model achieved superior performance in two out of three subsets: normal and dusty-air, with mIoU of 35.8 and 31.6, respectively. However, our model shows lower performance in low-illumination subset, with mIoU of 25.2.

However, traditional train-based approaches are specialized for the style variation on which they were trained, becoming highly vulnerable when the domains differ. To illustrate this, we conducted additional experiments testing models on different domains from the ones they were trained on. Specifically, we tested the baseline model trained on a particular subset of ChangeSim on the other subsets. The experimental results are shown in Table 2. The baseline model, being specialized for their in-domain data, suffers performance drops when the data changes, indicating a lack of generalization. Specifically, when the baseline model trained on the dusty-air subset is tested on the same dataset, it achieves a performance score of 29.7. However, when the model is trained on the normal or low-illumination datasets and tested on the dusty-air dataset, the performance scores are relatively lower, at 27.2 and 27.1, respectively. This performance drop is also observed in other subsets. This is a major weakness of the baseline in performing the task of change detection, as they are vulnerable to changes in the data. Conversely, our approach, not being tailored to any specific domain, avoids the performance drop typically associated with changes in the dataset In other words, our model can be applied to all subsets without the need for retraining each time the environment changes.

We present qualitative results in Figure 5. These results show that our approach effectively performs change detection without training. More qualitative results and ablation studies will be provided in the supplementary material.

5 Conclusion

In this paper, we present a novel approach to zero-shot Scene Change Detection (SCD). Our method performs SCD without training by leveraging a tracking model. To adapt the tracking model for SCD, we introduce two training-free components: the style bridging layer and the adaptive content threshold. Our model demonstrates robustness across various environmental changes, showcasing its versatility. We believe our work offers a fresh perspective on SCD and represents a significant step forward in its practical application.

Limitations. While our model benefits from not requiring a training process, it incurs a relatively higher computational cost during inference compared to existing methods. This increased inference cost arises because our model employs two networks. Future work could focus on enhancing speed by utilizing lighter networks or consolidating certain procedures to improve.

Zero-Shot Scene Change Detection

Supplementary Material

A   Implementation Details

A.1   Details on Mask Generation

This section explains how to create a mask for input into the tracking model. We use Segment Anything Model (SAM) [17] to generate the mask proposal. We executed SAM's automatic mask generation pipeline with the parameters set as shown in the Table 3.

Hyperparameter	Value
SAM model	vit_h
points_per_side	32
pred_iou_thresh	0.86
stability_score_thresh	0.92
crop_n_layers	1
crop_n_points_downscale_factor	2
min_mask_region_area	100

Table 3: Hyperparameters of SAM.

Meanwhile, the masks generated by SAM possess two characteristics that make them unsuitable for our task. First, there are too many small masks. Second, a single pixel can belong to multiple masks. Since the change in scene change detection (SCD) occurs at the object level, the mask size should correspond to the object level and not be too small. Additionally, each pixel in the image can only belong to one object, so it must belong to at most one mask. Therefore, we conducted the following post-processing steps:

Through this process, each pixel belongs to at most one mask, and masks that are too small are naturally removed.

Step	Details
1	Run the Segment Anything Model (SAM) to obtain masks.
2	Sort the SAM masks from smallest to largest area.
3	Overlay the sorted masks in order. This process ensures that if one pixel belongs to multiple masks, the largest mask among them is selected.
4	For each mask, if the ratio of the area covered by the overlaid mask is more than 50%, it is merged with the largest mask among the overlaid masks. This process removes the masks that occluded most of the area through step 3.
5	For the VL-CMU-CD [29] dataset, remove the masks that do not contain any information. These are the black areas at the edges of the images.

Table 4: Mask generation process.

A.2   Details on Tracking Model

We use DEVA [13] for our tracking model. We used the DEVA structure with only one modification, incorporating style bridging layers (SBL) within the encoder architecture. The first SBL is

positioned immediately after the first convolutional layer, while subsequent SBLs are placed after the addition operation within each residual block [24].

DEVA parameters were set as follows.

Hyperparameter	Value
detection_every	5
voting_frames	3
max_missed_detection_count	5
max_num_objects	200

Table 5: Hyperparameters of DEVA.

B Additional Experiments

We show additional experimental results on the VL-CMU-CD [29] and PCD [2] dataset.

B.1 Dataset and metric

VL-CMU-CD [29] is a dataset that includes information on urban street view changes over a long period, encompassing seasonal variations. Following the baseline approach, we performed predictions using 512×512-sized images. As the change class in this dataset is limited to a binary classification of the 'missing' class, we used only the 'missing' class for our three types of prediction.

PCD [2] is a dataset consisting of panoramic images and includes two subsets: GSV and TSUNAMI. Following the baselines, we performed predictions on reshaped images of size 256×1024. Each data point is classified into binary change or unchanged categories. We consider the detected new, missing, and replaced predictions into a 'changed' class for evaluation.

Evaluation Metrics. Following the previous work, we used the F1 score for evaluation.

B.2 Experimental Results

Table 6 presents the experimental results with other state-of-the-art. The baseline model performs well when the training and test datasets are the same, but its performance drops sharply when the datasets change, indicating its sensitivity to the dataset. Since change detection must operate across various seasons and weather conditions in real-world scenarios, robustness to style changes is essential for effective change detection. This sensitivity implies that the baseline model is overfitted to the limited style changes present in the specific dataset. In contrast, our approach remains robust across all style changes.

VL-CMU-CD & PCD				
			Test set	
Method	Trained Set	VL-CMU-CD	PCD	Average
C-3PO [16]	VL-CMU-CD	**79.4**	11.6	45.5
	PCD	24.3	**82.4**	53.4
Ours	-	51.6	56.5	**54.0**

Table 6: **Experimental results on VL-CMU-CD and PCD.** Results are expressed in the F1 score. The baseline model performs best when the training and test are identical. However, its performance greatly declines when these sets differ. Conversely, our method does not exhibit this issue.

C   Ablation Experiments

We conducted ablation experiments to show the effectiveness of our approach. All experiments were conducted on the ChangeSim dataset [6].

Config.		ChangeSim			
ACT	SBL	Normal	Dust	Dark	Average
		28.2	24.4	25.0	25.9
	✓	27.1	27.0	**25.7**	26.6
✓		**36.0**	18.1	21.6	25.3
✓	✓	35.8	**31.6**	25.2	**30.9**

Table 7: Ablation study on ACT and SBL.

Addressing Content gap and Style gap. We evaluate the effectiveness of the proposed adaptive content threshold (ACT) and style bridging layer (SBL). As shown in Table 7, experimental results indicate that the combined use of ACT and SBL yields the highest average performance. Additionally, these experiments offer interesting observations: 1. SBL is effective when the style of reference and query image differ (i.e., dusty-air and low-illumination subset), but its effectiveness diminishes in subsets with consistent styles (i.e., normal subset). 2. ACT demonstrates its efficacy particularly when the model's tracking performance is high (e.g., normal subset). In experiments where tracking performance is poor (e.g., low-illumination subset), the addition of ACT leads to a decline in performance.

SBL	ChangeSim			
	Normal	Dust	Dark	Average
0	36.0	18.1	21.6	25.3
1	35.7	29.2	23.9	29.6
2	**36.1**	31.1	24.7	30.6
3	36.0	31.5	25.0	30.8
4	35.8	**31.6**	**25.2**	**30.9**

Table 8: Ablation study on the number of SBL.

The number of SBL. We experiment to determine the optimal number of SBL required. We progressively add SBL from the early layer of the encoder. As mentioned in the previous section, the initial Style Bridging Layer (SBL) was placed directly after the first convolutional layer. The following SBLs were inserted after the addition operation within each residual block. As shown in Table 8, experimental results indicate that applying SBL to all blocks of the encoder yields the best performance.

T_{max}	ChangeSim			
	Normal	Dust	Dark	Average
1	33.6	28.9	22.2	28.2
30	35.6	**31.6**	24.4	30.5
60	**35.8**	31.6	25.2	**30.9**
90	35.6	31.2	**25.6**	30.8
unlimited	33.3	30.5	25.6	29.8

Table 9: Ablation study on the length of the sequence T_{max}.

The length of Sequence. We conduct experiments under various T_{max} values. As shown in Table 9, our method shows a significant improvement when extended to video compared to before the extension ($T_{max} = 1$). However, it is notable that increasing T_{max} does not consistently lead to improved

performance; increasing the video length beyond 60 has little to no impact on performance or may even lead to a decline.

T_{max}	Content Threshold	ChangeSim			
		Normal	Dust	Dark	Average
1	0.05	33.6	28.9	22.2	28.2
	0.4	31.9	24.6	18.4	25.0
	Adaptive	**33.6**	**28.9**	**22.2**	**28.2**
30	0.05	31.1	29.9	**26.2**	29.1
	0.4	35.4	31.3	23.9	30.2
	Adaptive	**35.6**	**31.6**	24.4	**30.5**
60	0.05	30.0	29.0	**26.5**	28.5
	0.4	35.8	31.5	25.2	30.8
	Adaptive	**35.8**	**31.6**	25.2	**30.9**

Table 10: Ablation study on Adaptive Content Threshold.

The Adaptive Content Threshold. To illustrate the necessity of varying the content threshold according to the sequence length, we conducted experiments across three different sequence lengths. The three sequence lengths were 1, 60, and 30, which are the T_{max} for image-level SCD, our standard T_{max} for video, and an intermediate value, respectively. The fixed threshold values were set to 0.05 and 0.4, approximating the values of ACT when $T_{max} = 1$ and $T_{max} = 60$, respectively.

As shown in Table 10, when the sequence length is 1, a threshold of 0.05 performs the best, while performance is poor at a threshold of 0.4. Conversely, for sequence lengths of 30 and 60, a threshold of 0.05 results in the lowest performance, while higher thresholds improve performance. Furthermore, the results indicate that the ACT consistently achieves the best performance across all sequence lengths. This shows the validity and effectiveness of ACT.

D   Qualitative Results

We present additional qualitative results in Figures 6, 7, 8, and 9 to show the effectiveness of our approach across various datasets. To enhance understanding, detailed images of the intermediate processes are also provided. During the intermediate process, identical masks before and after tracking are represented by the same color. Specifically, the same colored masks in M^r and $M^{r \rightarrow q}$ denote the same object mask, and the same applies to M^q and $M^{q \rightarrow r}$. However, since M^r and M^q do not share a tracking relationship, the same color between these two images holds no relationship.

The qualitative results show that our approach effectively identifies new and missing objects, and generates the final prediction accurately.
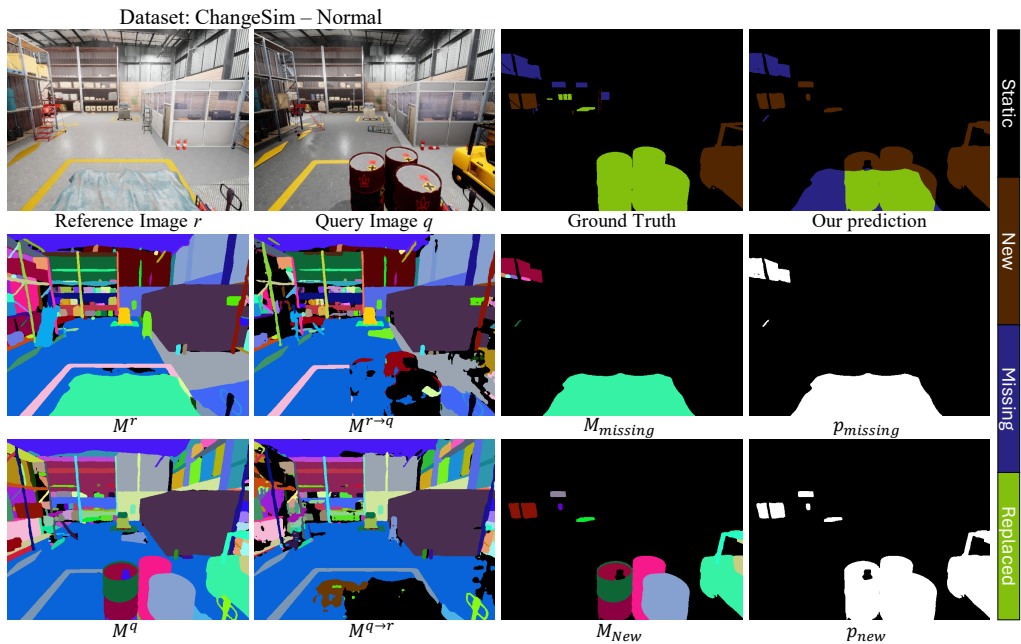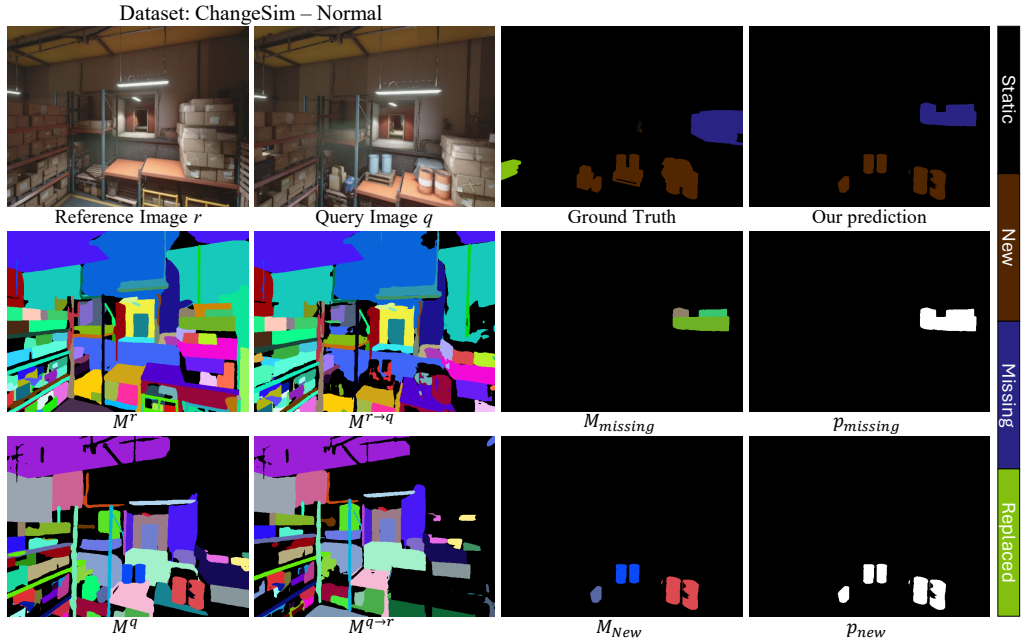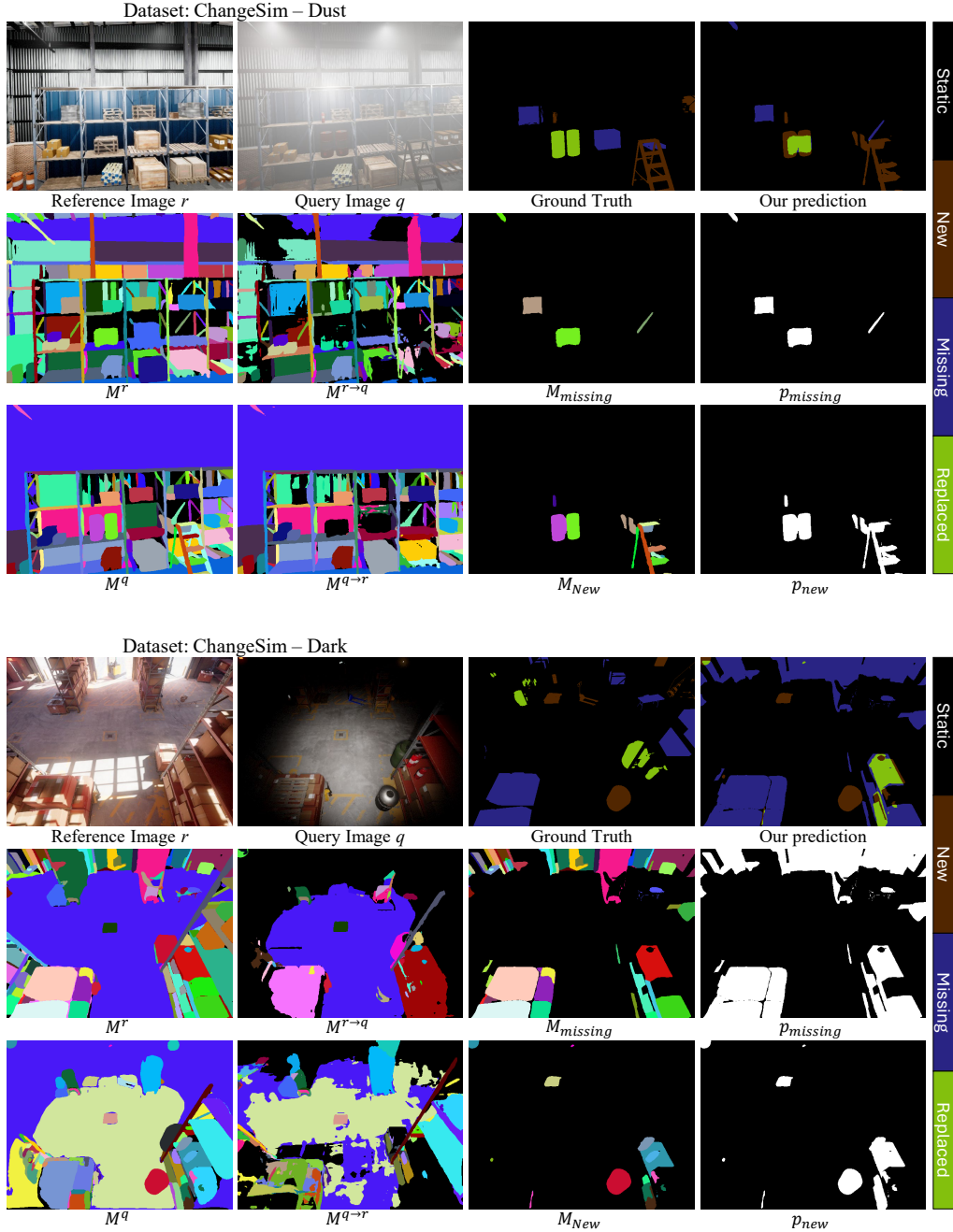
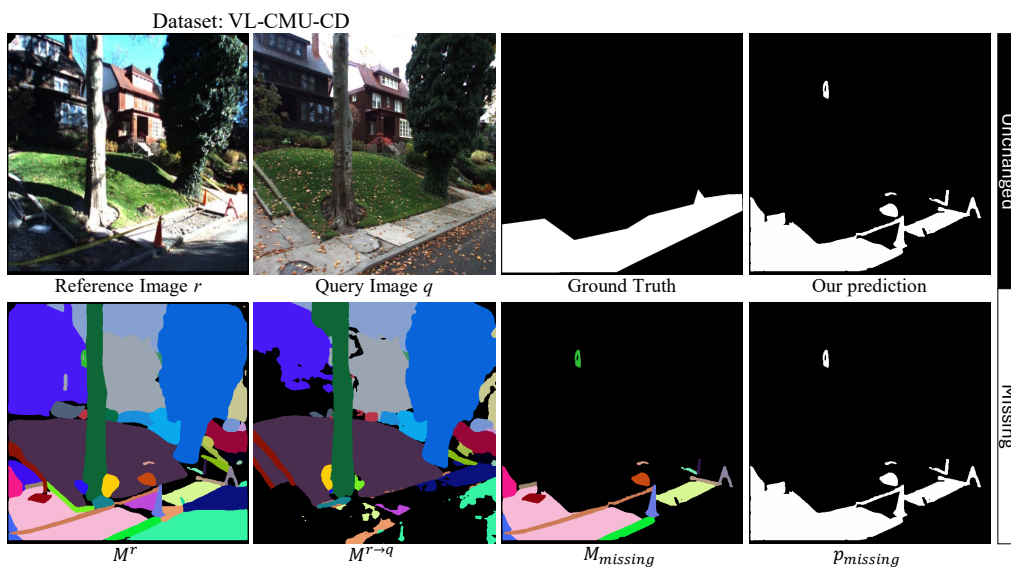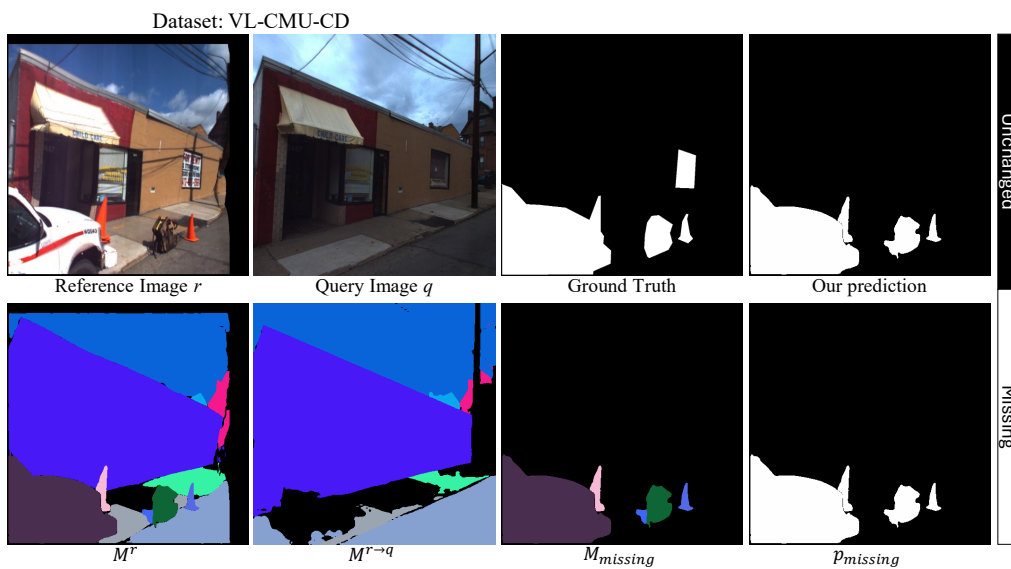Figure 6: **Qualitative Results on ChangeSim-Normal.**

Figure 7: **Qualitative Results on ChangeSim-Dark and ChangeSim-Dust.**

Figure 8: **Qualitative Results on VL-CMU-CD [29].**

Dataset: PCD

Reference Image r — Query Image q

Unchanged / Changed

Ground Truth — Our prediction

M^r — $M^{r \to q}$

M^q — $M^{q \to r}$

$M_{missing}$ — M_{New}

Dataset: PCD

Reference Image r — Query Image q

Unchanged / Changed

Ground Truth — Our prediction

M^r — $M^{r \to q}$

M^q — $M^{q \to r}$
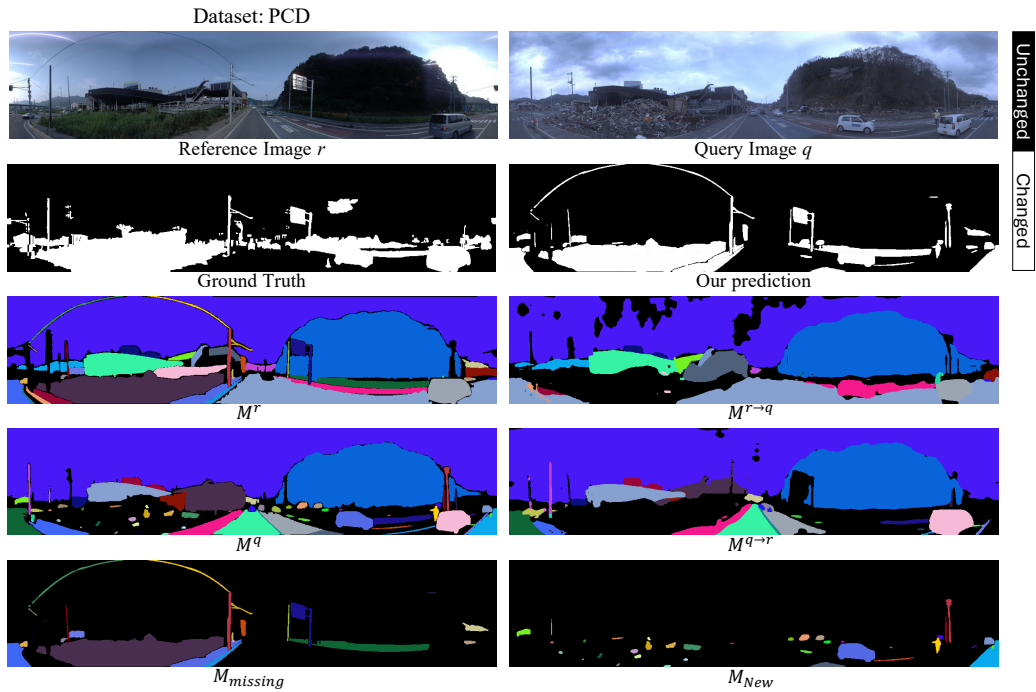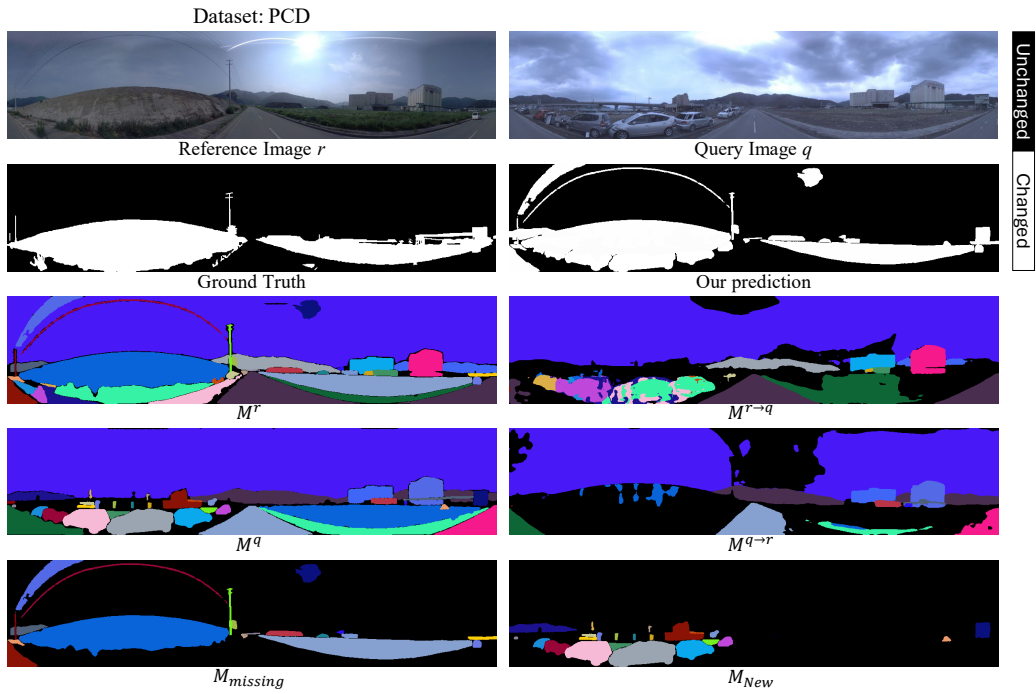
$M_{missing}$ — M_{New}

Figure 9: **Qualitative Results on PCD [2].**

References

[1] K. Sakurada, T. Okatani, and K. Deguchi. Detecting changes in 3d structure of a scene from multi-view images captured by a vehicle-mounted camera. In *Proceedings of the IEEE Conference on Computer Vision and Pattern Recognition (CVPR)*, pages 137–144, 2013.

[2] K. Sakurada and T. Okatani. Change detection from a street image pair using cnn features and superpixel segmentation. In *British Machine Vision Conference (BMVC)*, 2015.

[3] Z. Lv, H. Huang, W. Sun, M. Jia, J. A. Benediktsson, and F. Chen. Iterative training sample augmentation for enhancing land cover change detection performance with deep learning neural network. *IEEE Transactions on Neural Networks and Learning Systems*, 2023.

[4] F. Song, T. Dan, R. Yu, K. Yang, Y. Yang, W. Chen, X. Gao, and S.-H. Ong. Small uav-based multi-temporal change detection for monitoring cultivated land cover changes in mountainous terrain. *Remote sensing letters*, 10(6):573–582, 2019.

[5] A. Agarwal, S. Kumar, and D. Singh. Development of neural network based adaptive change detection technique for land terrain monitoring with satellite and drone images. *Defence Science Journal*, 69(5):474, 2019.

[6] J.-M. Park, J.-H. Jang, S.-M. Yoo, S.-K. Lee, U.-H. Kim, and J.-H. Kim. Changesim: Towards end-to-end online scene change detection in industrial indoor environments. In *2021 IEEE/RSJ International Conference on Intelligent Robots and Systems (IROS)*, pages 8578–8585. IEEE, 2021.

[7] J.-M. Park, U.-H. Kim, S.-H. Lee, and J.-H. Kim. Dual task learning by leveraging both dense correspondence and mis-correspondence for robust change detection with imperfect matches. In *Proceedings of the IEEE/CVF Conference on Computer Vision and Pattern Recognition*, pages 13749–13759, 2022.

[8] S. Lee and J.-H. Kim. Semi-supervised scene change detection by distillation from feature-metric alignment. In *Proceedings of the IEEE/CVF Winter Conference on Applications of Computer Vision (WACV)*, pages 1226–1235, 2024.

[9] C. Sun, J. Wu, H. Chen, and C. Du. Semisanet: A semi-supervised high-resolution remote sensing image change detection model using siamese networks with graph attention. *Remote Sensing*, 14(12):2801, 2022.

[10] M. Seo, H. Lee, Y. Jeon, and J. Seo. Self-pair: Synthesizing changes from single source for object change detection in remote sensing imagery. In *Proceedings of the IEEE/CVF Winter Conference on Applications of Computer Vision (WACV)*, pages 6374–6383, 2023.

[11] Y. Furukawa, K. Suzuki, R. Hamaguchi, M. Onishi, and K. Sakurada. Self-supervised simultaneous alignment and change detection. In *2020 IEEE/RSJ International Conference on Intelligent Robots and Systems (IROS)*, pages 6025–6031, 2020.

[12] R. Sachdeva and A. Zisserman. The change you want to see. In *Proceedings of the IEEE/CVF Winter Conference on Applications of Computer Vision (WACV)*, 2023.

[13] H. K. Cheng, S. W. Oh, B. Price, A. Schwing, and J.-Y. Lee. Tracking anything with decoupled video segmentation. In *Proceedings of the IEEE/CVF International Conference on Computer Vision (ICCV)*, pages 1316–1326, 2023.

[14] H. K. Cheng and A. G. Schwing. Xmem: Long-term video object segmentation with an atkinson-shiffrin memory model. In *European Conference on Computer Vision (ECCV)*, pages 640–658. Springer, 2022.

[15] S. Chen, K. Yang, and R. Stiefelhagen. Dr-tanet: Dynamic receptive temporal attention network for street scene change detection. In *2021 IEEE Intelligent Vehicles Symposium (IV)*, pages 502–509. IEEE, 2021.

[16] G.-H. Wang, B.-B. Gao, and C. Wang. How to reduce change detection to semantic segmentation. *Pattern Recognition*, 138:109384, 2023.

[17] A. Kirillov, E. Mintun, N. Ravi, H. Mao, C. Rolland, L. Gustafson, T. Xiao, S. Whitehead, A. C. Berg, W.-Y. Lo, et al. Segment anything. In *Proceedings of the IEEE/CVF International Conference on Computer Vision (ICCV)*, pages 4015–4026, 2023.

[18] Z. Peng, Q. Tian, J. Xu, Y. Jin, X. Lu, X. Tan, Y. Xie, and L. Ma. Generalized category discovery in semantic segmentation. *arXiv preprint arXiv:2311.11525*, 2023.

[19] V. Maquiling, S. A. Byrne, D. C. Niehorster, M. Nyström, and E. Kasneci. Zero-shot segmentation of eye features using the segment anything model (sam). *Proceedings of the ACM on Computer Graphics and Interactive Techniques*, 7(2):1–16, 2024.

[20] Y. Cheng, L. Li, Y. Xu, X. Li, Z. Yang, W. Wang, and Y. Yang. Segment and track anything. *arXiv preprint arXiv:2305.06558*, 2023.

[21] Z. Yang and Y. Yang. Decoupling features in hierarchical propagation for video object segmentation. *Advances in Neural Information Processing Systems*, 35:36324–36336, 2022.

[22] F. Rajič, L. Ke, Y.-W. Tai, C.-K. Tang, M. Danelljan, and F. Yu. Segment anything meets point tracking. *arXiv preprint arXiv:2307.01197*, 2023.

[23] X. Huang and S. Belongie. Arbitrary style transfer in real-time with adaptive instance normalization. In *Proceedings of the IEEE International Conference on Computer Vision (ICCV)*, pages 1501–1510, 2017.

[24] K. He, X. Zhang, S. Ren, and J. Sun. Deep residual learning for image recognition. In *Proceedings of the IEEE Conference on Computer Vision and Pattern Recognition (CVPR)*, pages 770–778, 2016.

[25] T. Karras, S. Laine, and T. Aila. A style-based generator architecture for generative adversarial networks. In *Proceedings of the IEEE/CVF Conference on Computer Vision and Pattern Recognition (CVPR)*, pages 4401–4410, 2019.

[26] Z. Wu, X. Wang, J. E. Gonzalez, T. Goldstein, and L. S. Davis. Ace: Adapting to changing environments for semantic segmentation. In *Proceedings of the IEEE/CVF International Conference on Computer Vision (ICCV)*, pages 2121–2130, 2019.

[27] Q. Xu, R. Zhang, Y.-Y. Wu, Y. Zhang, N. Liu, and Y. Wang. Simde: A simple domain expansion approach for single-source domain generalization. In *Proceedings of the IEEE/CVF Conference on Computer Vision and Pattern Recognition (CVPR)*, pages 4797–4807, 2023.

[28] S. Thrun. Probabilistic robotics. *Communications of the ACM*, 45(3):52–57, 2002.

[29] P. F. Alcantarilla, S. Stent, G. Ros, R. Arroyo, and R. Gherardi. Street-view change detection with deconvolutional networks. *Autonomous Robots*, 42:1301–1322, 2018.